ACS Chemical Neuroscience

pubs.acs.org/chemneuro Research Article

Molecular Mechanism for the Allosteric Inhibition of the Human Serotonin Transporter by Antidepressant Escitalopram

Weiwei Xue,* Tingting Fu, Shengzhe Deng, Fengyuan Yang, Jingyi Yang, and Feng Zhu*

Cite This: ACS Chem. Neurosci. 2022, 13, 340−351 Read Online

ACCESS | Metrics & More | Article Recommendations | Supporting Information

ABSTRACT: Human serotine transporter (hSERT) is one of the most influential drug targets, and its allosteric modulators (e.g., escitalopram) have emerged to be the next-generation medication for psychiatric disorders. However, the molecular mechanism underlying the allosteric modulation of hSERT is still elusive. Here, the simulation strategies of conventional (cMD) and steered (SMD) molecular dynamics were applied to investigate this molecular mechanism from distinct perspectives. First, cMD simulations revealed that escitalopram's binding to hSERT's allosteric site simultaneously enhanced its binding to the orthosteric site. Then, SMD simulation identified that the occupation of hSERT's allosteric site by escitalopram could also block its dissociation from the orthosteric site. Finally, by comparing the simulated structures of two hSERT−escitalopram complexes with and without allosteric modulation, a new conformational coupling between an extracellular (Arg104-Glu494) and an intracellular (Lys490-Glu494) salt bridge was identified. In summary, this study explored the mechanism underlying the allosteric modulation of hSERT by collectively applying two MD simulation strategies, which could facilitate our understanding of the allosteric modulations of not only hSERT but also other clinically important therapeutic targets.

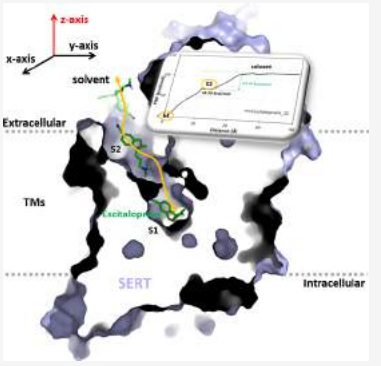

KEYWORDS: *serotonin transporter, allostery, escitalopram, molecular dynamics, drug design*

INTRODUCTION

Serotonin (5-hydroxytryptamine, 5-HT) signaling in the brain influences sleep, mood, cognition, and pain.[1−3] Imbalances of serotonin homeostasis can lead to psychiatric disorders that seriously affect the normal life of people.[4−6] Serotonin transporter (SERT) plays an essential role in the reuptake of serotonin from extracellular space into neurons.[7] Particularly, it is an important target of FDA-approved antidepressants such as selective serotonin reuptake inhibitors (SSRIs).[6,8] SERT belongs to the family of Na^+/Cl^- neurotransmitter transporters (NTTs)[9] and is composed of 12 transmembrane domains (TMs) connected by intracellular and extracellular loops (ILs and ELs).[7] X-ray crystal structure of human SERT showed that it contains 5 + 5 inverted-topological repeats, formed by TM1 to TM5 and TM6 to TM10.[1]

Although SSRIs are the most prescribed class of drugs used for the treatment of many psychiatric disorders,[4] the delayed onset of action and adverse effects such as sexual dysfunction limit patient acceptance of these medications.[10−17] To discover novel therapeutics, several efforts toward the structure and function of SERT were performed.[6,18−20] Based on the crystal structures of SERT,[1] bacterial leucine transporter (LeuT),[21] and *Drosophila* dopamine transporter (dDAT),[21] site mutagenesis[22−26] and computational modeling[27−31] revealed SSRI binding at the orthosteric site (S1) formed by TM1, 3, 6, 8, and 10. The models were confirmed by the cocrystal structures of human SERT complexed with SSRIs with diverse scaffolds at the S1 site,[32] which represent a milestone in the field of membrane transport and provide blueprints for future drug design.[1,33−39]

In addition to the S1 site, the recently solved X-ray structure of SERT confirmed the existence of an allosteric site (S2) in the transport.[1,31,40,41] The S2 site was found residing at the periphery of the extracellular vestibule in human SERT (Figure 1), which opens up a new way of designing novel allosteric medicines to overcome the delayed onset of action and serious side effects of conventional antidepressants targeting the S1 site of SERT.[42−48] Furthermore, biochemical and structural biology data indicated that the fast onset of action and high efficacy of escitalopram (SSRI) were related to the allosteric mechanism of action.[1,40,49−51] The crystal structures provide glimpses of escitalopram in complex with the SERT.[1] However, the biophysical, thermodynamic, and kinetic properties, as well as critical conformational coupling underlying the allosteric modulation that is essential for the clinical efficacy are still not fully understood.[52] Moreover, the lack of allosteric compounds with high binding affinity limited the pharmaco-

Received: October 21, 2021
Accepted: January 4, 2022
Published: January 18, 2022

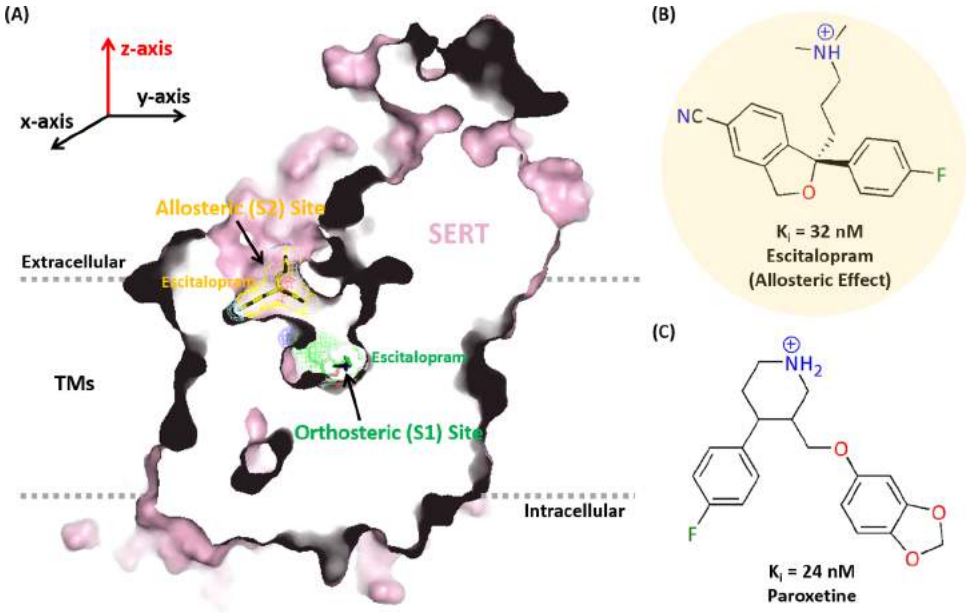

Figure 1. Protein and ligand structures and related information used in this study. (A) X-ray crystal structure of human SERT bound to two escitalopram molecules simultaneously at the orthosteric (S1) and allosteric (S2) sites (PDB code: 5I73). The protein is shown in a purple cartoon surface. Binding of two escitalopram molecules at the S1 and S2 sites is represented in green and orange sticks, respectively. The orientation of the protein in membrane was calculated on the OPM server, and the *x*, *y*, and *z* dimensions of the studied complex coordinates are shown in the top left of the graph. Chemical structures and binding affinities of two clinically used antidepressants escitalopram (B) and paroxetine (C) with and without allosteric effect.

logical implications of the SERT allosteric inhibition.[44,53] To better understand the allosteric inhibition mechanism of the SERT by escitalopram, experimental data should well complement computational modeling approaches such as molecular dynamics (MD),[6] which has a widespread application in determining how a stimulus at one site on a protein causes effects in other sites at an atomistic level.[54−57]

In this study, comprehensive molecular dynamics (MD) simulations were performed to investigate the molecular mechanism of allosteric regulation in the SERT. Starting from the crystal structures, the pharmacodynamics profiles of SERT complexed with two clinically used antidepressants were characterized by the conventional MD (cMD) approach. The two clinically used antidepressants are escitalopram and paroxetine. Escitalopram cooperatively binds to orthosteric and allosteric sites of SERT, while paroxetine only binds to the orthosteric site of SERT.[1] The estimated binding free energies in the equilibrated states indicated that simultaneous binding of escitalopram in the S2 will enhance the binding affinity of the drug in the S1 site of the protein. Furthermore, the pathways of the two drugs dissociated from the SERT were predicted by the steered MD (SMD) method. Compared with paroxetine that only binds to the S1 site, the calculated potentials of mean force (PMFs) showed that there are two energy platforms along the drug unbinding pathway of escitalopram from the S1 site of SERT.

RESULTS AND DISCUSSION

Equilibrium States of Drugs' Binding in SERT. Recently, co-crystallized structures of human SERT bound to escitalopram and paroxetine have been solved.[1] They provided good starting points to sample the conformations of each complex in an explicit membrane environment by the cMD simulation.[58] As shown in Figure S1, all of the studied systems reached converged after a relatively short time (~20 ns) simulation (Figure S1). The flexibility of the extracellular and intracellular loops (ELs and ILs) is the main cause of the relatively significant RMSD fluctuations in each system, which is further monitored by the per-residue RMSF of the protein (Figure S2). As expected, the average RMSD values of the systems indicated that the conformations of ligand as well as residues located at the S2 site are more flexible than that of the S1 site (Table S1). For example, the RMSD of ligand (1.75 Å) and binding residues (1.40 Å) refering to the S2 site were larger than that of the S1 site (the values for ligand and binding residues were 0.71 and 0.67 Å, respectively). Moreover, when escitalopram is simultaneously bound to S1 and S2 sites, the decreased conformational flexibilities of the two binding sites (Figure S2 and Table S1) suggest a cooperative binding mechanism.

Unbinding Processes of Drugs from SERT. To provide quantitative estimation of the nonequilibrated unbinding processes of drugs, the pathways of escitalopram and paroxetine dissociated from the S1 or S2 site of SERT along the defined reaction coordinate (RC) of the z-axis direction (Figure 1) were investigated by SMD simulation. The convergence of SMD simulation can be judged by the amount of sampling controlled by the number of simulation trajectories and the pulling velocity.[59] In this work, 10 randomized SMD trajectories were collected for each system to efficiently sample the conformations of the unbinding processes of drugs.[60] For a simulation, the slower the velocity, the closer the process is to being reversible.[59] Here, a pulling velocity of 0.001 Å/ps was adopted to pull escitalopram and paroxetine out from their binding sites in SERT, which was 10 times slower than that used in several other research systems.[61] Therefore, the simulation trajectories were run for 40 ns for the S1 site ligand and for 30 ns for the S2 site ligand because of the lengths for different pathways (Figure 2).

https://doi.org/10.1021/acschemneuro.1c00694
ACS Chem. Neurosci. 2022, 13, 340−351

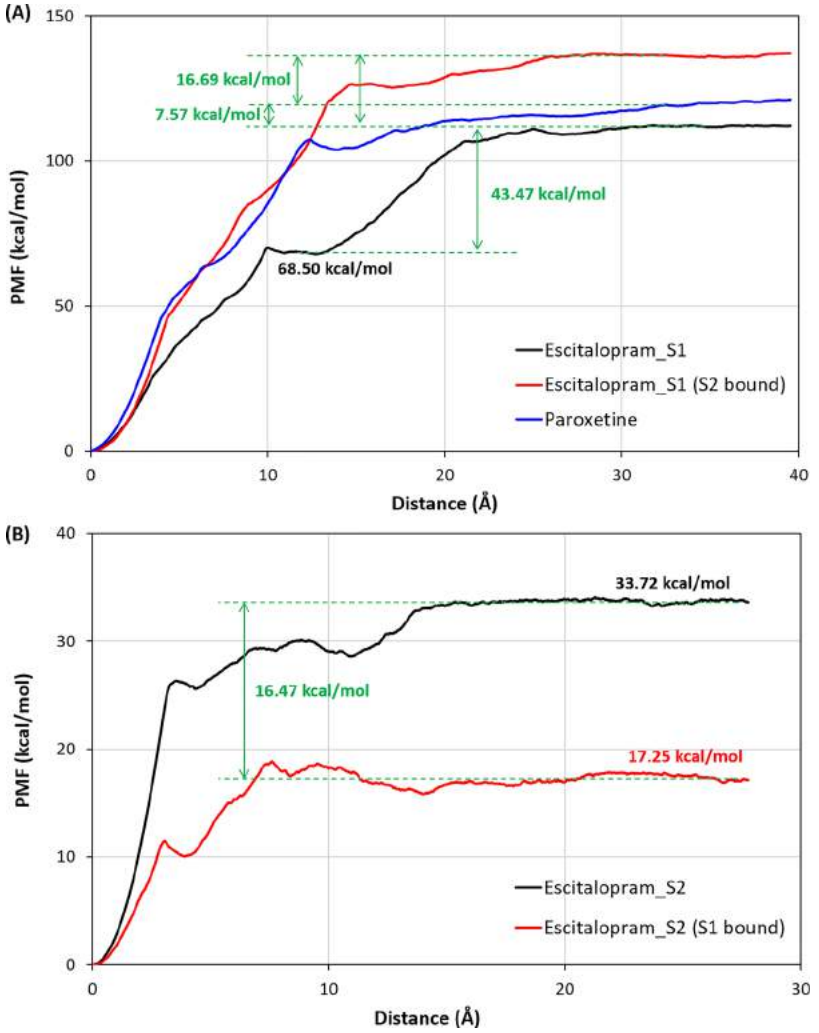

Figure 2. Potentials of mean force (PMF) profiles of drugs dissociated from S1 and S2 sites of SERT. (A) The value of escitalopram dissociated from the S1 site (111.97 kcal/mol) was lower than that of paroxetine (119.54 kcal/mol), and the PMF of escitalopram dissociated from the S1 site increased to 136.23 kcal/mol when the S2 site was occupied by a second escitalopram. (B) The PMF value of escitalopram dissociated from the S2 site (33.72 kcal/mol) was higher than the case that the S1 site was occupied by another escitalopram (17.25 kcal/mol).

Thermodynamics and Kinetics Profiles for the (Un)-binding States of Drugs. *Free Energies of Drug Binding to SERT at the Equilibrium States.* The binding free energy is generally used in drug design to characterize the binding strength of a drug to its target. Based on MD equilibrium trajectory, endpoint binding free energy calculated by the MM/GBSA method[62] has been widely used to explore the details of diverse protein−ligand interactions. To further understand the interactions between the two studied drugs (escitalopram and paroxetine) and SERT, the binding free energies (ΔG_{calc}) of the designed four different complexes were estimated by the MM/GBSA method. As shown in Table 2, the ΔG_{calc} values of escitalopram and paroxetine at the S1 site were −48.85 and −49.97 kcal/mol, respectively, corrected well with the trend of the experimental values (−10.23 and −10.40 kcal/mol for escitalopram and paroxetine, respectively). Moreover, the decomposed energy terms (Table S2) can help us to understand the features of complex formation:[63−65] the gas-phase energies (ΔE_{vdW} and ΔE_{ele}) mainly contribute to the interactions, and the polar solvation energy (ΔG_{pol}) was unfavorable for the formation of the complexes, which is consistent with previous studies.[28,48,57,66]

In Table 2, the binding free energies of escitalopram to S1 or S2 sites in the other two designed simulation systems were also obtained, which is a good complement to the current experimental result. The values of ΔG_{calc} indicated that the binding of escitalopram at the S1 site was more tight when the S2 site was occupied. In contrast, for the S2 site, ΔG_{calc} suggested that escitalopram bound to the S2 site more tightly when there is no ligand bound at the S1 site. Those estimated binding free energies of different systems not only elucidated the experimental phenomena that the binding affinity of escitalopram at S1 could be enhanced by the binding of the second escitalopram at the S2 site,[1] but also showed that escitalopram has a higher binding selectivity to the S1 site.[44] Nevertheless, the estimated higher binding affinity of escitalopram at the S2 site of SERT when the S1 site was empty implied that the S2 site has the potential of strong plasticity to be targeted by small molecules.

Potential of Mean Forces along the Unbinding Pathways of Drugs from SERT. For each system, the PMF involved in the unbinding pathway of drug from SERT was reconstructed (Figure 2). As shown in Figure 2, the PMF of escitalopram dissociated from the S1 site (111.97 kcal/mol) was lower than

https://doi.org/10.1021/acschemneuro.1c00694
ACS Chem. Neurosci. 2022, 13, 340−351

Table 1. Designed Systems for Conventional and Steered Molecular Dynamics Simulations

drugs	targets	PDB code	environment	sMD (ns)	SMD (ns)
escitalopram	SERT (S1-S2)	5I73 with T110A, I91A, and T439S mutated back to native structure	POPC, TIP3P water	100	10 × 40
	SERT (S1)	5I71 with T110A, I91A, and T439S mutated back to native structure	POPC, TIP3P water	100	10 × 40
	SERT (S2)	5I71 with the S1 site escitalopram removed and T110A, I91A, and T439S mutated back to native structure	POPC, TIP3P water	100	10 × 30
paroxetine	SERT (S1)	5I6X with T110A, I91A, and T439S mutated back to the native structure	POPC, TIP3P water	100	10 × 40

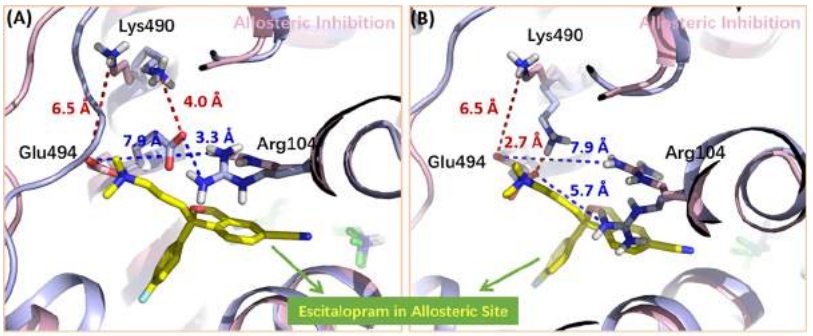

	Extracellular Gate Arg104 (OE1) - Glu494 (NH1)	Intracellular Gate Lys490 (NZ) - Glu494 (NH1)
Escitalopram_S1 (S2 bound)	7.9 Å	6.5 Å
Escitalopram_S1	3.3 Å	4.0 Å
Paroxetine_S1	5.7 Å	2.7 Å

Figure 3. Conformations coupling of the two salt bridges located at extracellular and intracellular accessible regions of SERT. The conformations of SERT bound to (A) escitalopram or (B) paroxetine in orthosterically inhibited state (light blue) were superimposed to the structure of SERT bound to escitalopram in the allosterically inhibited state (light pink). The monitored distances of the two salt bridges are listed in the inserted table. OE1, NH1, and NZ represent the types of atoms used for measuring the salt bridge distance.

that of paroxetine (119.54 kcal/mol), and the trend of the values is consistent with their activities in SERT.[67] However, when the S2 site was occupied by a second escitalopram, the PMF of escitalopram dissociated from the S1 site increased to 136.23 kcal/mol, which is 7.57 and 16.69 kcal/mol higher than escitalopram and paroxetine, respectively, in the case S2 site was empty. As a result, the calculated PMFs provide a good illustration of the drug efficacy data from clinical cases.[49,50,68,69]

In addition, as the value of PMF is inversely proportional to the drug dissociation rate (k_{off}),[70] the kinetics profiles of drugs unbinding from SERT can be estimated using the PMFs obtained by SMD simulation trajectories. The PMF values of the three systems in Figure 2A demonstrated that escitalopram exhibited the slowest dissociation rate from the S1 site when the S2 site was occupied by a second escitalopram. Meanwhile, the estimated dissociation time of escitalopram and paroxetine from the S1 site was verified by the available experimental data.[44] Thus, it can propose that a second escitalopram binds at the S2 site and leads to the longer residence time ($1/k_{off}$) of escitalopram at the S1 site, which is the main reason for its higher therapeutic efficacy.

Moreover, the PMFs of escitalopram dissociated from the S2 site are shown in Figure 2B. In consistence with the trend of estimated binding strength (Table 2), the PMF value of escitalopram dissociated from the S2 site was higher when the S1 site was empty. In other words, the escitalopram exhibited a relatively longer residence time at the S2 site in the absence of escitalopram at the S1 site. This finding was similar to a previous study that SMD simulation of the substrate translocation pathway of LeuT (the prototype for SERT) identified a second substrate-binding site (refers to S2 in this study) targeted by tricyclic antidepressants.[71] SERT is a 12-transmembrane protein and the S1 and S2 sites located at the middle and extracellular vestibule of the protein, respectively. Compared to the PMFs of escitalopram dissociated from the S2 site (17.25 and 33.72 kcal/mol with and without the S1 site occupied, respectively), the higher value for escitalopram dissociated from the S1 site (111.97 kcal/mol) could be understood by the relative positions of the two sites in SERT.

Hence, all of the evidence from thermodynamics and kinetics analysis, as well as the homologous protein suggested that the S2 site of SERT could be considered as a target for novel drug design, and this new target had been confirmed by the recently developed escitalopram analogues.[44]

Molecular Mechanism for the Allosteric Inhibition of SERT by Escitalopram. *Conformational Coupling of SERT from Orthostericcally to Allosterically Inhibited States.* After structural refinements of the designed complexes (Table 1) by cMD in a mimicked physiological environment,[72] the representative conformation of each complex was derived from the equilibrium trajectory (Figure S3). For the drugs binding at the S1 site (Figure S3A−C), the binding modes were consistent with the reported crystallographic and computational studies.[28,32] For example, the salt bridge between the negatively charged oxygen atom of Asp98 and the positively charged nitrogen atoms of escitalopram and

https://doi.org/10.1021/acschemneuro.1c00694
ACS Chem. Neurosci. 2022, 13, 340−351

Table 2. Calculated and Experimental Binding Free Energies of Studied Drugs to Targets

drugs	targets		ΔG_{calc} (kcal/mol)[a]	ΔG_{exp} (kcal/mol)[b]	K_i (nM)[b]
escitalopram	SERT (S1)[c]		−48.85 ± 2.46	−10.23	32
	SERT (S2)[d]		−38.57 ± 3.07	[f]	
	SERT (S1-S2)[e]	S1	−50.38 ± 2.71		
		S2	−36.91 ± 2.35	−7.16	5800 (IC_{50})
paroxetine	SERT(S1)[c]		−49.97 ± 2.59	−10.40	24

[a]Estimated MM/GBSA binding free energy (ΔG_{calc}) with standard deviations. [b]Experimental binding free energy (ΔG_{exp}) based on K_i[67] or IC_{50}[44] values using $\Delta G = RT\ln(K_i)$ or $\Delta G \approx RT\ln(IC_{50})$. [c]Drug binding to the orthosteric (S1) site of SERT. [d]Drug binding to the allosteric (S2) site of SERT. [e]Drug simultaneously binding to the S1 and S2 sites of SERT. [f]No experimental data reported.

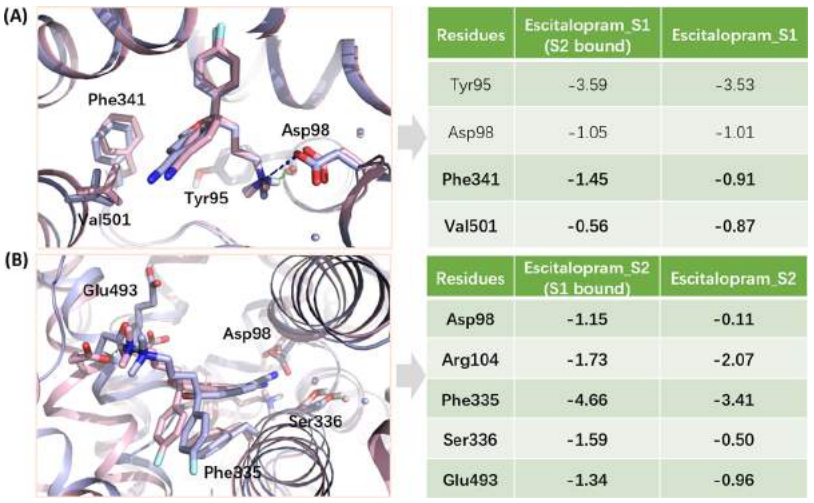

Residues	Escitalopram_S1 (S2 bound)	Escitalopram_S1
Tyr95	-3.59	-3.53
Asp98	-1.05	-1.01
Phe341	-1.45	-0.91
Val501	-0.56	-0.87

Residues	Escitalopram_S2 (S1 bound)	Escitalopram_S2
Asp98	-1.15	-0.11
Arg104	-1.73	-2.07
Phe335	-4.66	-3.41
Ser336	-1.59	-0.50
Glu493	-1.34	-0.96

Figure 4. Interaction energy coupling analysis. The residues contributed differently to escitalopram binding from orthosterically to allosterically inhibited states were mapped to the (A) S1 and (B) S2 binding sites of SERT.

paroxetine played a crucial role in the recognition of the drugs in the S1 site of SERT. For the S2 site located at the extracellular vestibule of the transporter, escitalopram mainly interacted with 12 residues around the pocket: Asp98, Arg104, Ala331, Gln332, Phe335, Ser336, Glu493, Glu494, Pro499, Leu502, Ile552, and Phe556 (Figure S3D,E), and 50% of them have been verified by site mutagenesis experiment,[50,73,74] such as the residues Glu494 and Phe556 formed hydrogen bond and hydrophobic interactions with escitalopram. Recently, vilazodone was found to be an allosteric inhibitor of SERT,[74] and the allosteric site residues Arg104, Gln332, Phe335, Glu493, Glu494, Tyr495, Glu497, Pro499, Phe556, Ser559, Pro560, Pro561, and Tyr579 were discovered to interact with vilazodone. Although there are seven common residues (Arg104, Gln332, Phe335, Glu493, Glu494, Pro499, and Phe556), the extensive hydrophobic site (Tyr495, Pro499, Ser559, Pro560, Pro561, and Tyr579) was not found in our study due to the molecular size difference between escitalopram and vilazodone.

To further characterize the allosteric effect of escitalopram on the conformational behaviors of SERT, those derived from representative conformations of complexes in orthosterically and allosterically inhibited states are aligned in Figure 3. A closer view of the binding modes shows the conformational coupling of the two binding sites. In allosterically inhibited state, the measured distances of the two salt bridges at extracellular (Arg104 (OE1)−Glu494 (NH1)) and intracellular (Lys490 (NZ)−Glu494 (NH1)) accessible regions were 7.9 and 6.5 Å, respectively, while in orthosterically inhibited states, the corresponding distances were 3.3 and 4.0 Å for the escitalopram-bound complex, and 5.7 and 2.7 Å for the paroxetine-bound complex (Figure 3). The OE1, NH1 and NZ represent the atoms types of the residues used for calculating the salt bridge distance.

Therefore, the identified binding modes as well as conformational coupling here provided useful information for deeply understanding the two sites at different states, which could be used for the design of compounds having higher binding selectivity toward the S2 site.[44]

Interaction Energy Coupling from Orthosterically to Allosterically Inhibited States of SERT. In addition to the conformational coupling of the residues forming salt bridges at the extracellular and intracellular region,[50,73] it is valuable to explore the energy coupling of residues in the S1 and S2 sites of SERT. Compared with paroxetine, ΔG_{calc} estimated from cMD showed that escitalopram at the S2 site enhanced its binding affinity to the S1 site, while the activity of escitalopram at the S2 site decreased when the S1 site was occupied (Table 2). To understand this coupling effect, ΔG_{calc} was further decomposed into per-residue of the transporter (Table S3). The residues contributed differently to escitalopram binding were mapped to the topology structure of SERT (Figure 4). In the inset table of Figure 4, residues Asp98, Arg104, Phe335, Ser336, Phe341, Glu493, and Val501 at the S1 or S2 sites were identified to be involved in the interaction energy coupling. Therefore, complementary to the previous structural and site mutagenesis studies,[50,73] the detailed interaction energy data at the per-residue level in this work provided quantitative characterization of S1 and S2 site residues by comparing the orthosterically to allosterically inhibited states of SERT by escitalopram, enabling the rational design of new compounds with similar or different effects.[54]

https://doi.org/10.1021/acschemneuro.1c00694
ACS Chem. Neurosci. 2022, 13, 340−351

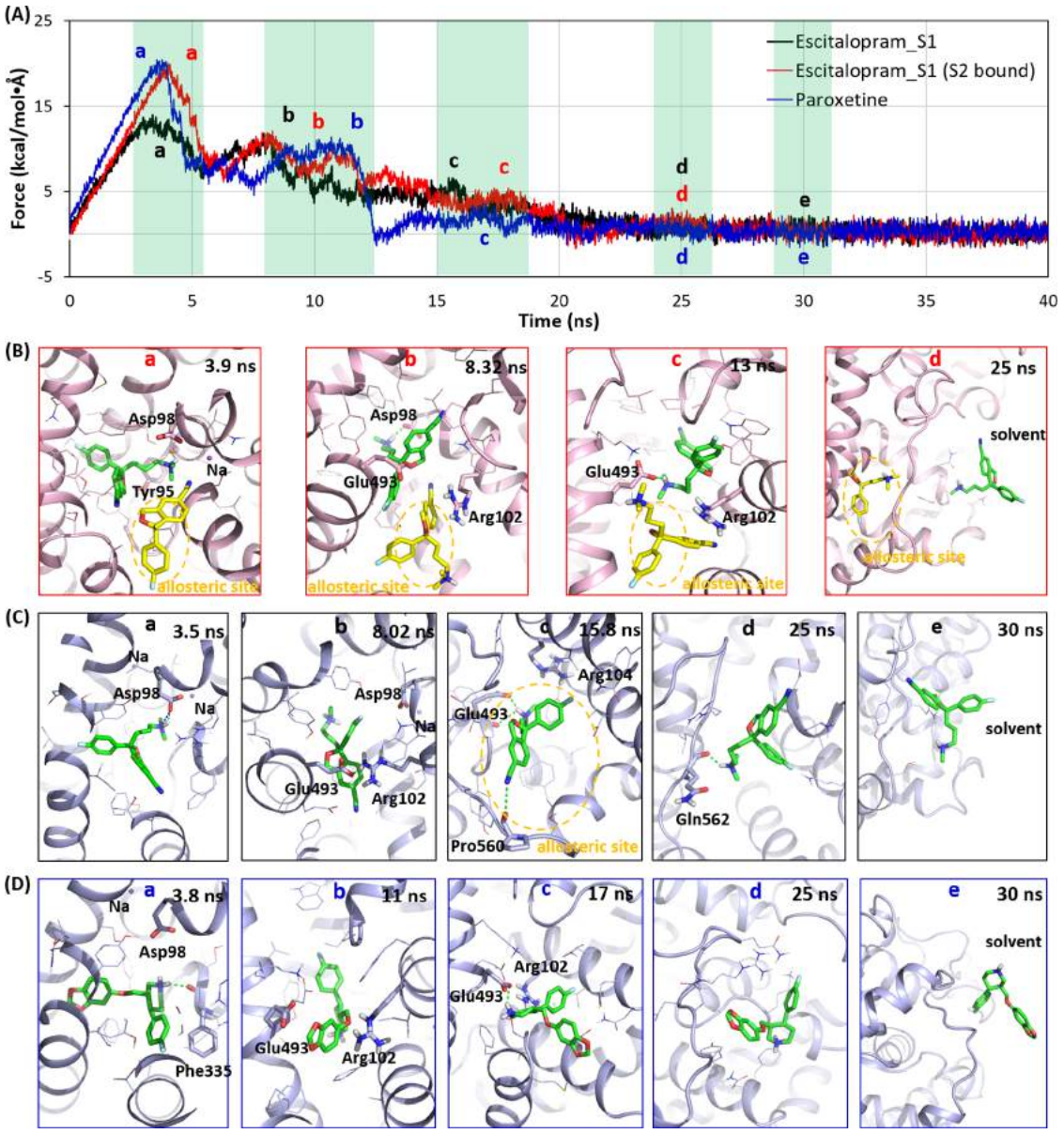

Figure 5. Applied force and intermediate snapshots of each system during the simulation. (A) Force vs time of escitalopram and paroxetine dissociated from the S1 site of SERT during SMD simulations. The drugs were pulled at 0.001 Å/ps using a time step of 2 fs. (B–D) Extracted snapshots for the relative positions of drug and transporter along the unbinding pathways for escitalopram (red boxes a–d), escitalopram (S2 bound) (black boxes a–e), and paroxetine (blue boxes a–e). The SERT and drugs are displayed in cartoon and stick representation, respectively. The salt bridge and hydrogen bond are shown in blue and green dashed lines, respectively.

Dissociation of Escitalopram from the S1 Site of SERT Was Blocked by the Allosteric Inhibition. The PMF curve from SMD illustrated the different pathways of escitalopram and paroxetine dissociating from the S1 site or the S2 site of SERT (Figure 2). According to the force profiles applied during the simulation (Figure 5A), several specific snapshots were derived to show the crucial steps along the reaction coordinates (Figure 5B–D), which is useful for understanding the biological process of drugs dissociating from proteins.[60,75] Figure 5A shows that the applied force in all systems had a steady increase and reached a maximum when pulling the drug from the equilibrium state (in the first 4 ns). At this stage, escitalopram or paroxetine formed strong contacts with residues in the S1 site, such as the salt bridge between Asp98 and the drugs (box a in Figure 5B–D) and other hydrophobic interactions (Figure S3A–C). The maximum force for escitalopram (S2 bound) and paroxetine is apparently higher than that of escitalopram, which elucidated that the former were more tightly confined within the S1 site.[1]

On the other hand, the variation of the typical force profiles (Figure 5A) demonstrated that the drugs unbinding from the S1 site in different ways. In the allosterically inhibited simulation, escitalopram dissociated from S1 skirted around the S2 site and enters the solvent (boxes b–d in Figure 5B). In the case of orthosterically inhibited simulation, the S2 site was identified (box c in Figure 5C), which was consistent with the identified second binding site along the substrate translocation pathway of LeuT (the prototype for SERT) by SMD simulations.[71] Moreover, the flat energy basin of PMF curve for escitalopram in orthosterically inhibited simulation (Figure 2A) suggested that escitalopram dissociated from SERT by a two-step mechanism: (i) escitalopram moved away from the

https://doi.org/10.1021/acschemneuro.1c00694
ACS Chem. Neurosci. 2022, 13, 340–351

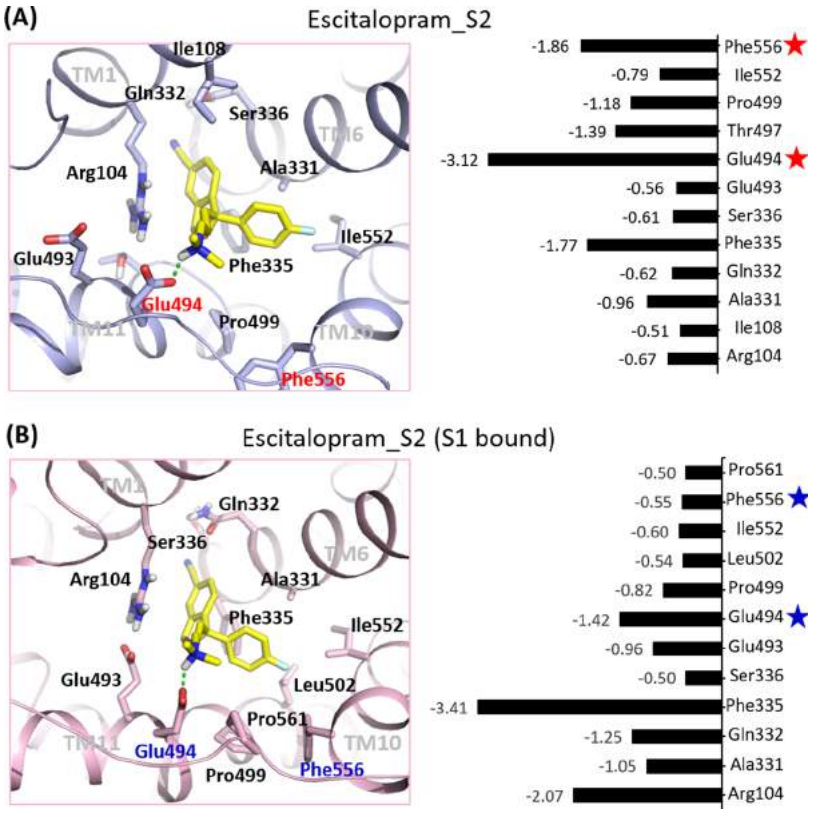

Figure 6. Structure and energy profiles of escitalopram bound to the S2 site of SERT in the cases of (A) empty and (B) occupied S1 site. The SERT and drug are displayed as cartoon and stick representation, respectively. Hydrogen bond is shown in the green dashed line.

S1 site and entered the S2 site (boxes a−c in Figure 5C) and (ii) the drug formed new hydrogen bonds with Glu493 and Pro560 in the S2 site; however, the hydrogen bonds were broken with the movement of escitalopram from the S2 site to the solvent (boxes c and d in Figure 5C). Thus, it can be learned from the simulations that the relative stability of escitalopram in the S2 site prevented its dissociation from the S1 site, which was in good consistence with experimental observation.[44] Compared with escitalopram, paroxetine basically dissociated from the S1 site through a one-step mechanism (Figures 2 and 5D), which helped us to further understand the biochemical test that paroxetine has no binding affinity to the S2 site of SERT.[76]

Potential of the S2 Site in SERT as a Therapeutic Target for Novel Drug Design. In vivo studies show that escitalopram interacting with the S2 site in SERT has higher efficacy and faster onset of action.[77] However, whether the S2 site of SERT could be used as a potential therapeutic target for novel drug design, two questions should be addressed: (i) how to increase the binding affinities of compounds to the S2 site and (ii) how to modify the compounds' selective binding between S1 and S2 sites.[48,78,79]

The structural alignment of escitalopram binding at SERT S2 site before and after MD simulation is shown in Figure S4. As the initial structure of escitalopram bound to the S2 site of SERT was constructed based on the crystal structure of SERT complexed with escitalopram simultaneously at the S1 and S2 sites, except for the eight common interaction residues (Ile108, Asp328, Gln332, Glu494, Pro499, Ser555, Phe556, and Pro560), significant conformational changes occurred for escitalopram and the corresponding binding site residues (Tyr495, Ile553, and Gln562). Interestingly, the estimated binding free energies of escitalopram to SERT showed that the drug bound more tightly at the S2 site when the S1 site was empty (Table 2), which implies that the S2 site has the potential of strong plasticity to be targeted by small molecules. In addition, the PMF values of escitalopram dissociated from the S2 site of SERT revealed that the drug had a relatively longer residence time at the S2 site in the absence of escitalopram at the S1 site (Figure 2B). Nevertheless, compared with the drugs binding at the S1 site, both the thermodynamics and kinetics profiles of the compound binding at the S2 site should be further improved.[44,73] The simulation results indicated that there are 12 important residues contributed to escitalopram binding to SERT in the S2 site (Table S3). The analysis of binding modes as well as key residues' energy contributions demonstrated that Glu494 in TM11 and Phe556 in TM10 played an important role in the recognition of escitalopram with the S2 site (Figure 6). Therefore, we proposed that an extended S2 site including the escitalopram binding site and the TM10 and TM11 segments near the S2 site could be considered to design more potent allosteric inhibitors of SERT. And the structurally and sequentially distinctive TM11 segment in MATs could be exploited for the structure-based design of selective compounds toward the S2 site.[80] SMD simulation showed that a large force (Figure S5A) was needed to break the hydrogen bond between Gln562 and cyano group of escitalopram during the drug dissociation from the S2 site (box **a** in Figure S5B,C), which was confirmed by the conclusion that the group is absolutely essential for the escitalopram and its analogues to carry an allosteric potential.[44] Although several compounds binding to S2 were reported in recent years, most of them were based on the scaffold of escitalopram, which had low affinity

https://doi.org/10.1021/acschemneuro.1c00694
ACS Chem. Neurosci. 2022, 13, 340−351

and poor selectivity to the S2 site of SERT.[44,79,81] To solve these challenging problems, current computer-assisted drug design approaches such as in silico high-throughput screening and machine learning[82] are expected to discover a novel scaffold based on the specific conformation of the S2 site as well as the known compounds such as escitalopram and vilazodone.[46,74,83]

CONCLUSIONS

In this work, the detailed molecular mechanism of the binding and unbinding of two clinically used antidepressants (escitalopram and paroxetine) against S1 or S2 sites in human SERT was carefully characterized by comprehensive MD simulation. Results showed that escitalopram was able to bind to the S2 site of SERT and prevent the dissociation of the drug from the S1 site. Furthermore, comparison of the PMFs of the two antidepressants along their unbinding pathways as well as the binding free energies at the equilibrium states demonstrated the druggability of the S2 site in SERT. Moreover, the identification of key residues Glu494 and Phe556 is important for the recognition of escitalopram in the S2 site. These results provide detailed thermodynamics, kinetic properties, and critical conformational and energetic coupling insights into the molecular mechanism for the allosteric inhibition of SERT by escitalopram, which can be used to facilitate the discovery and design of novel drug for the treatment of mood disorders.

MATERIALS AND METHODS

Systems Preparation. *Preparation of the Crystallographic Structures.* Escitalopram and paroxetine are the first two drugs in which the binding modes of SSRIs in the SERT were revealed by crystallographic experiments.[1] Compared with paroxetine, the allosteric effect of escitalopram to SERT was discovered at a high concentration.[49,50] In this study, to explore the molecular mechanism of the allosteric regulation of escitalopram to SERT, four simulation complexes were designed (Table 1). There were the crystal structures of SERT complexed with escitalopram simultaneously at the S1 and S2 sites (PDB code: 5I73), escitalopram at the S1 site (PDB code: 5I71), paroxetine at the S1 site (PDB code: 5I6X), and escitalopram at the S2 site by removing the S1 site escitalopram in 5I73. Three mutations (T110A, I291A, and T439S) in the crystal structure of SERT were mutated back to its native state using the mutagenesis tool in PyMOL.

Construction of Protein–Ligand/Membrane Systems. The prepared four complexes were then preoriented in OPM and inserted into an explicit POPC lipid bilayer by means of Membrane Builder module in CHARMM-GUI. The TIP3P water of 40 Å thickness was placed above and below the constructed bilayer. The Na^+ and Cl^- counterions were used to neutralize the systems at an environmental salt concentration of 0.15 M. For each system, a periodic box with dimensions of ∼102 Å × 102 Å × 160 Å was generated, resulting in a system size of ∼130 000 atoms.

Force Field Parameters. LEaP was used to assign force field parameters for each partner of the complex, and the SERT protein, POPC liquids, Na^+ and Cl^- ions, and TIP3P waters were described using AMBER ff14SB,[84] Lipid14,[85] and monovalent ion parameters for TIP3P water, respectively. The parameters for escitalopram and paroxetine were created by Antechamber using general AMBER force field (GAFF)[86] and restrained electrostatic potential (RESP) partial charges.[87] Geometric optimization and the electrostatic potential calculations of ligands were performed at the HF/6-31G* level of Gaussian09 suite.

Molecular Dynamics Simulations. *Conventional Molecular Dynamics Simulation.* For each system, to remove bad contacts between the solute and solvent water molecules, energy minimization and equilibration simulations were carefully accomplished in three segments before production simulation. First, except for the lipid tail, all atoms were fixed to minimize 100 ps and equilibrate 500 ps. Second, each system with ligand heavy atoms, protein Cα atoms, and fixed ions was further minimized for 100 ps and equilibrated for 500 ps. Third, the entire system was all released to carry out 5 ns equilibrated simulation. Finally, a 100 ns production simulation without any restraints was conducted in the NPT ensemble at a temperature of 310 K and a pressure of 1 bar.

Steered Molecular Dynamics Simulation. Starting from the representative snapshots of the last 10 ns equilibrated cMD trajectory, one of the most popularly used enhanced sampling MD methods SMD was employed to sample the drug unbinding pathways from SERT using the constant velocity approach along the defined reaction coordinate of the z-axis direction (Figure 1). The pulling force was applied directly to the drugs, and the residues around 12 Å of the ligand were restrained by a harmonic potential with a constant force of 5 kcal/(mol·A^2). To ensure the validity of the stiff-spring approximation, the spring constant (k) was set to 500 pN/Å,[59] and a slow pulling velocity (v) of 0.001 Å/ps was used. For SMD simulations, pulling was stopped when the drugs were separated ∼25 Å from the edges of protein along the z-dimension, and 10 times replicated simulations were conducted for each system.

All MD simulations were carried out with GPU-accelerated NAMD software. During simulations, periodic boundary conditions were employed and electrostatic calculations were based on the particle-mesh Ewald (PME) method with a 10 Å nonbonded cutoff. An integration step of 2 fs was used and the coordinates of trajectory were saved every 10 ps. Hydrogen atoms were constrained using the SHAKE algorithm.

Thermodynamics Analysis. *Endpoint Binding Free Energy.* Molecular mechanics/generalized Born surface area (MM/GBSA) method[88] was employed to calculate the endpoint binding free energy ($\Delta G_{MM/GBSAcalc}$) between SERT and escitalopram or paroxetine. The method has been successfully applied to rank the relative binding free energy of small molecules in membrane proteins.[26,28,48,89,90] In this work, using the 1000 snapshots extracted from the last 30 ns equilibrium MD trajectory, ΔG_{calc} was estimated as below.

$$\Delta G_{calc} = \Delta E_{vdW} + \Delta E_{ele} + \Delta G_{pol} + \Delta G_{nonpol} \quad (1)$$

The terms ΔE_{vdW} and ΔE_{ele} represent the van der Waals and electrostatic interaction energies in the gas phase, respectively. ΔG_{pol} and ΔG_{nonpol} are the polar and nonpolar solvation energies, respectively. ΔE_{vdW} and ΔE_{ele} were calculated using the AMBER force field ff14SB.[84] The free energy of polar solvation (ΔG_{pol}) was calculated by the modified GB model (igb = 2), and solute and solvent dielectric constants were set to 2 and 80, respectively. The free energy of nonpolar solvation (ΔG_{nonpol}) was calculated by ΔG_{nonpol} = 0.0072 × ΔSASA, and ΔSASA was estimated by the LCPO method with 1.4 Å Probe radii.

Per-Residue Basis Energy Contribution. To quantitatively investigate the contribution of each residue to the binding free energy and energetic coupling between the S1 and S2 sites, energy decomposition analysis was performed on a per-residue basis. Per-residue decomposition calculates the energy contribution of single residues by summing its interactions over all residues in the system. Except for the nonpolar solvation energy determined by the ICOSA method, the calculation of the gas-phase interactions and the solvation energies was similar to that in eq 1.

Potential of Mean Force. Based on the 10 replicated trajectories from SMD simulations, the PMFs for drugs dissociated from proteins were calculated using the second-order cumulant expansion formula of Jarzynski's equality according to eq 2.

$$\langle e^{-\beta W} \rangle = e^{-\beta \Delta F} \quad (2)$$

where $\beta = 1/k_B T$ is the inverse temperature and k_B is the Boltzmann constant, w is the external work done on the system during the process, and ΔF is the Helmholtz free energy difference. The average $\langle \cdot \rangle$ is over repeated realizations of the process.[59]

https://doi.org/10.1021/acschemneuro.1c00694
ACS Chem. Neurosci. 2022, 13, 340−351

■ ASSOCIATED CONTENT

Supporting Information

The Supporting Information is available free of charge at https://pubs.acs.org/doi/10.1021/acschemneuro.1c00694.

RMSD and RMSF values; total and decomposed terms of binding energies as well as per-residues energy contribution; representative snapshots of the drugs bound and dissociated from the S1 and/or S2 site of SERT; and force vs time of escitalopram dissociated from the S2 site of SERT during SMD simulations (PDF)

■ AUTHOR INFORMATION

Corresponding Authors

Weiwei Xue − *Chongqing Key Laboratory of Natural Product Synthesis and Drug Research, Innovative Drug Research Center, School of Pharmaceutical Sciences, Chongqing University, Chongqing 401331, China; Central Nervous System Drug Key Laboratory of Sichuan Province, Luzhou 646000, China;* orcid.org/0000-0002-3285-0574; Phone: +86-023-6567-8450; Email: xueww@cqu.edu.cn

Feng Zhu − *Chongqing Key Laboratory of Natural Product Synthesis and Drug Research, Innovative Drug Research Center, School of Pharmaceutical Sciences, Chongqing University, Chongqing 401331, China; College of Pharmaceutical Sciences, Zhejiang University, Hangzhou 310058, China; Innovation Institute for Artificial Intelligence in Medicine of Zhejiang University, Alibaba-Zhejiang University Joint Research Center of Future Digital Healthcare, Hangzhou 330110, China;* orcid.org/0000-0001-8069-0053; Phone: +86-571-8820-8444; Email: zhufeng@zju.edu.cn

Authors

Tingting Fu − *Chongqing Key Laboratory of Natural Product Synthesis and Drug Research, Innovative Drug Research Center, School of Pharmaceutical Sciences, Chongqing University, Chongqing 401331, China*

Shengzhe Deng − *Chongqing Key Laboratory of Natural Product Synthesis and Drug Research, Innovative Drug Research Center, School of Pharmaceutical Sciences, Chongqing University, Chongqing 401331, China*

Fengyuan Yang − *Chongqing Key Laboratory of Natural Product Synthesis and Drug Research, Innovative Drug Research Center, School of Pharmaceutical Sciences, Chongqing University, Chongqing 401331, China*

Jingyi Yang − *Chongqing Key Laboratory of Natural Product Synthesis and Drug Research, Innovative Drug Research Center, School of Pharmaceutical Sciences, Chongqing University, Chongqing 401331, China*

Complete contact information is available at: https://pubs.acs.org/10.1021/acschemneuro.1c00694

Author Contributions

W.X. and F.Z. designed the research. W.X. and T.F. performed the research. W.X., T.F., S.D., F.Y., J.Y., and F.Z. analyzed the data. W.X. and F.Z. wrote the manuscript.

Funding

Funded by the Entrepreneurship and Innovation Support Plan for Chinese Overseas Students of Chongqing (cx2020127); Fundamental Research Fund for Central Universities (2019CDYGYB005, 2018QNA7023); National Natural Science Foundation of China (21505009, 81872798 & U1909208); Open Project of Central Nervous System Drug Key Laboratory of Sichuan Province (200019-01SZ); Natural Science Foundation of Zhejiang Province (LR21H300001); Leading Talent of the "Ten Thousand Plan"—National High-Level Talents Special Support Plan of China; "Double Top-Class" University Project (181201*194232101); and Key R&D Program of Zhejiang Province (2020C03010). This work was supported by Westlake Laboratory (Westlake Laboratory of Life Sciences and Biomedicine); Alibaba-Zhejiang University Joint Research Center of Future Digital Healthcare; Alibaba Cloud; and Information Technology Center of Zhejiang University.

Notes

The authors declare no competing financial interest.

■ ABBREVIATIONS

SERT, serotonin transporter; SSRIs, selective serotonin reuptake inhibitors; TMs, transmembrane domains; ILs and ELs, intracellular and extracellular loops; LeuT, leucine transporter; dDAT, *Drosophila* dopamine transporter; S1, orthosteric site; MD, molecular dynamics; SMD, steered MD; PMF, potentials of mean force; GAFF, general AMBER force field; RESP, restrained electrostatic potential; MM/GBSA, molecular mechanics/generalized Born surface area; RMSD, root-mean-square deviation; RMSF, root-mean-square fluctuation; RC, reaction coordinate

■ REFERENCES

(1) Coleman, J. A.; Green, E. M.; Gouaux, E. X-ray structures and mechanism of the human serotonin transporter. *Nature* **2016**, *532*, 334−339.

(2) Yin, J.; Sun, W.; Li, F.; Hong, J.; Li, X.; Zhou, Y.; Lu, Y.; Liu, M.; Zhang, X.; Chen, N.; Jin, X.; Xue, J.; Zeng, S.; Yu, L.; Zhu, F. VARIDT 1.0: variability of drug transporter database. *Nucleic Acids Res.* **2020**, *48*, D1042−D1050.

(3) Fu, T.; Li, F.; Zhang, Y.; Yin, J.; Qiu, W.; Li, X.; Liu, X.; Xin, W.; Wang, C.; Yu, L.; Gao, J.; Zheng, Q.; Zeng, S.; Zhu, F. VARIDT 2.0: structural variability of drug transporter. *Nucleic Acids Res.* **2021**, D1417−D1431.

(4) Li, Y. H.; Yu, C. Y.; Li, X. X.; Zhang, P.; Tang, J.; Yang, Q.; Fu, T.; Zhang, X.; Cui, X.; Tu, G.; Zhang, Y.; Li, S.; Yang, F.; Sun, Q.; Qin, C.; Zeng, X.; Chen, Z.; Chen, Y. Z.; Zhu, F. Therapeutic target database update 2018: enriched resource for facilitating bench-to-clinic research of targeted therapeutics. *Nucleic Acids Res.* **2018**, *46*, D1121−D1127.

(5) Hong, J.; Luo, Y.; Zhang, Y.; Ying, J.; Xue, W.; Xie, T.; Tao, L.; Zhu, F. Protein functional annotation of simultaneously improved stability, accuracy and false discovery rate achieved by a sequence-based deep learning. *Briefings Bioinf.* **2020**, *21*, 1437−1447.

(6) Hong, J.; Luo, Y.; Mou, M.; Fu, J.; Zhang, Y.; Xue, W.; Xie, T.; Tao, L.; Lou, Y.; Zhu, F. Convolutional neural network-based annotation of bacterial type IV secretion system effectors with enhanced accuracy and reduced false discovery. *Briefings Bioinf.* **2020**, *21*, 1825−1836.

(7) Pramod, A. B.; Foster, J.; Carvelli, L.; Henry, L. K. SLC6 transporters: structure, function, regulation, disease association and therapeutics. *Mol. Aspects Med.* **2013**, *34*, 197−219.

(8) Zhang, S.; Amahong, K.; Zhang, C.; Li, F.; Gao, J.; Qiu, Y.; Zhu, F. RNA-RNA interactions between SARS-CoV-2 and host benefit viral development and evolution during COVID-19 infection. *Briefings Bioinf.* **2021**, No. bbab397.

(9) Kristensen, A. S.; Andersen, J.; Jorgensen, T. N.; Sorensen, L.; Eriksen, J.; Loland, C. J.; Stromgaard, K.; Gether, U. SLC6 neurotransmitter transporters: structure, function, and regulation. *Pharmacol. Rev.* **2011**, *63*, 585−640.

(10) Artigas, F. Future directions for serotonin and antidepressants. *ACS Chem. Neurosci.* **2013**, *4*, 5−8.
(11) Chen, L.; Zou, B.; Lee, V. H. F.; Yan, H. Analysis of the Relative Movements Between EGFR and Drug Inhibitors Based on Molecular Dynamics Simulation. *Curr. Bioinf.* **2018**, *13*, 299−309.
(12) Liao, Y.-d.; Jiang, Z.-r. MoABank: An Integrated Database for Drug Mode of Action Knowledge. *Curr. Bioinf.* **2019**, *14*, 446−449.
(13) Munir, A.; Malik, S. I.; Malik, K. A. Proteome Mining for the Identification of Putative Drug Targets For Human Pathogen Clostridium tetani. *Curr. Bioinf.* **2019**, *14*, 532−540.
(14) Srivastava, N.; Mishra, B. N.; Srivastava, P. In-Silico Identification of Drug Lead Molecule Against Pesticide Exposed-neurodevelopmental Disorders Through Network-based Computational Model Approach. *Curr. Bioinf.* **2019**, *14*, 460−467.
(15) Zhao, X.; Chen, L.; Guo, Z.-H.; Liu, T. Predicting Drug Side Effects with Compact Integration of Heterogeneous Networks. *Curr. Bioinf.* **2019**, *14*, 709−720.
(16) Yin, J.; Li, F.; Zhou, Y.; Mou, M.; Lu, Y.; Chen, K.; Xue, J.; Luo, Y.; Fu, J.; He, X.; Gao, J.; Zeng, S.; Yu, L.; Zhu, F. INTEDE: interactome of drug-metabolizing enzymes. *Nucleic Acids Res.* **2021**, *49*, D1233−D1243.
(17) Fu, J.; Zhang, Y.; Liu, J.; Lian, X.; Tang, J.; Zhu, F. Pharmacometabonomics: data processing and statistical analysis. *Briefings Bioinf.* **2021**, *22*, No. bbab138.
(18) Zeppelin, T.; Ladefoged, L. K.; Sinning, S.; Schiott, B. Substrate and inhibitor binding to the serotonin transporter: Insights from computational, crystallographic, and functional studies. *Neuropharmacology* **2019**, *161*, No. 107548.
(19) Sinning, S.; Musgaard, M.; Jensen, M.; Severinsen, K.; Celik, L.; Koldso, H.; Meyer, T.; Bols, M.; Jensen, H. H.; Schiott, B.; Wiborg, O. Binding and orientation of tricyclic antidepressants within the central substrate site of the human serotonin transporter. *J. Biol. Chem.* **2010**, *285*, 8363−8374.
(20) Tang, J.; Fu, J.; Wang, Y.; Li, B.; Li, Y.; Yang, Q.; Cui, X.; Hong, J.; Li, X.; Chen, Y.; Xue, W.; Zhu, F. ANPELA: analysis and performance assessment of the label-free quantification workflow for metaproteomic studies. *Briefings Bioinf.* **2020**, *21*, 621−636.
(21) Penmatsa, A.; Wang, K. H.; Gouaux, E. X-ray structure of dopamine transporter elucidates antidepressant mechanism. *Nature* **2013**, *503*, 85−90.
(22) Andersen, J.; Stuhr-Hansen, N.; Zachariassen, L.; Toubro, S.; Hansen, S. M.; Eildal, J. N.; Bond, A. D.; Bogeso, K. P.; Bang-Andersen, B.; Kristensen, A. S.; Stromgaard, K. Molecular determinants for selective recognition of antidepressants in the human serotonin and norepinephrine transporters. *Proc. Natl. Acad. Sci. U.S.A.* **2011**, *108*, 12137−12142.
(23) Wang, X.; Li, F.; Qiu, W.; Xu, B.; Li, Y.; Lian, X.; Yu, H.; Zhang, Z.; Wang, J.; Li, Z.; Xue, W.; Zhu, F. SYNBIP: synthetic binding proteins for research, diagnosis and therapy. *Nucleic Acids Res.* **2021**, D560−D570.
(24) Xue, W.; Yang, F.; Wang, P.; Zheng, G.; Chen, Y.; Yao, X.; Zhu, F. What contributes to serotonin-norepinephrine reuptake inhibitors' dual-targeting mechanism? The key role of transmembrane domain 6 in human serotonin and norepinephrine transporters revealed by molecular dynamics simulation. *ACS Chem. Neurosci.* **2018**, *9*, 1128−1140.
(25) Zhang, Y.; Ying, J. B.; Hong, J. J.; Li, F. C.; Fu, T. T.; Yang, F. Y.; Zheng, G. X.; Yao, X. J.; Lou, Y.; Qiu, Y.; Xue, W. W.; Zhu, F. How does chirality determine the selective inhibition of histone deacetylase 6? A lesson from Trichostatin A enantiomers based on molecular dynamics. *ACS Chem. Neurosci.* **2019**, *10*, 2467−2480.
(26) Fu, T.; Zheng, G.; Tu, G.; Yang, F.; Chen, Y.; Yao, X.; Li, X.; Xue, W.; Zhu, F. Exploring the binding mechanism of metabotropic glutamate receptor 5 negative allosteric modulators in clinical trials by molecular dynamics simulations. *ACS Chem. Neurosci.* **2018**, *9*, 1492−1502.
(27) Celik, L.; Sinning, S.; Severinsen, K.; Hansen, C. G.; Moller, M. S.; Bols, M.; Wiborg, O.; Schiott, B. Binding of serotonin to the human serotonin transporter. Molecular modeling and experimental validation. *J. Am. Chem. Soc.* **2008**, *130*, 3853−3865.
(28) Xue, W.; Wang, P.; Li, B.; Li, Y.; Xu, X.; Yang, F.; Yao, X.; Chen, Y. Z.; Xu, F.; Zhu, F. Identification of the inhibitory mechanism of FDA approved selective serotonin reuptake inhibitors: an insight from molecular dynamics simulation study. *Phys. Chem. Chem. Phys.* **2016**, *18*, 3260−3271.
(29) Abramyan, A. M.; Slack, R. D.; Meena, S.; Davis, B. A.; Newman, A. H.; Singh, S. K.; Shi, L. Computation-guided analysis of paroxetine binding to hSERT reveals functionally important structural elements and dynamics. *Neuropharmacology* **2019**, *161*, No. 107411.
(30) Davis, B. A.; Nagarajan, A.; Forrest, L. R.; Singh, S. K. Mechanism of Paroxetine (Paxil) Inhibition of the Serotonin Transporter. *Sci. Rep.* **2016**, *6*, No. 23789.
(31) Yang, Q.; Wang, Y.; Zhang, Y.; Li, F.; Xia, W.; Zhou, Y.; Qiu, Y.; Li, H.; Zhu, F. NOREVA: enhanced normalization and evaluation of time-course and multi-class metabolomic data. *Nucleic Acids Res.* **2020**, *48*, W436−W448.
(32) Coleman, J. A.; Gouaux, E. Structural basis for recognition of diverse antidepressants by the human serotonin transporter. *Nat. Struct. Mol. Biol.* **2018**, *25*, 170−175.
(33) Jakhar, R.; Dangi, M.; Khichi, A.; Chhillar, A. K. Relevance of Molecular Docking Studies in Drug Designing. *Curr. Bioinf.* **2020**, *15*, 270−278.
(34) Yang, Q.; Li, B.; Tang, J.; Cui, X.; Wang, Y.; Li, X.; Hu, J.; Chen, Y.; Xue, W.; Lou, Y.; Qiu, Y.; Zhu, F. Consistent gene signature of schizophrenia identified by a novel feature selection strategy from comprehensive sets of transcriptomic data. *Briefings Bioinf.* **2020**, *21*, 1058−1068.
(35) Liu, J.; Lian, X.; Liu, F.; Yan, X.; Cheng, C.; Cheng, L.; Sun, X.; Shi, Z. Identification of Novel Key Targets and Candidate Drugs in Oral Squamous Cell Carcinoma. *Curr. Bioinf.* **2020**, *15*, 328−337.
(36) Wang, J.; Wang, H.; Wang, X.; Chang, H. Predicting Drug-target Interactions via FM-DNN Learning. *Curr. Bioinf.* **2020**, *15*, 68−76.
(37) Adhikary, S.; Deredge, D. J.; Nagarajan, A.; Forrest, L. R.; Wintrode, P. L.; Singh, S. K. Conformational dynamics of a neurotransmitter:sodium symporter in a lipid bilayer. *Proc. Natl. Acad. Sci. U.S.A.* **2017**, *114*, E1786−E1795.
(38) Zhu, F.; Shi, Z.; Qin, C.; Tao, L.; Liu, X.; Xu, F.; Zhang, L.; Song, Y.; Liu, X.; Zhang, J.; Han, B.; Zhang, P.; Chen, Y. Therapeutic target database update 2012: a resource for facilitating target-oriented drug discovery. *Nucleic Acids Res.* **2012**, *40*, D1128−D1136.
(39) Yang, H.; Qin, C.; Li, Y. H.; Tao, L.; Zhou, J.; Yu, C. Y.; Xu, F.; Chen, Z.; Zhu, F.; Chen, Y. Z. Therapeutic target database update 2016: enriched resource for bench to clinical drug target and targeted pathway information. *Nucleic Acids Res.* **2016**, *44*, D1069−D1074.
(40) Zhu, R.; Sinwel, D.; Hasenhuetl, P. S.; Saha, K.; Kumar, V.; Zhang, P.; Rankl, C.; Holy, M.; Sucic, S.; Kudlacek, O.; Karner, A.; Sandtner, W.; Stockner, T.; Gruber, H. J.; Freissmuth, M.; Newman, A. H.; Sitte, H. H.; Hinterdorfer, P. Nanopharmacological Force Sensing to Reveal Allosteric Coupling in Transporter Binding Sites. *Angew. Chem., Int. Ed.* **2016**, *55*, 1719−1722.
(41) Tang, J.; Mou, M.; Wang, Y.; Luo, Y.; Zhu, F. MetaFS: performance assessment of biomarker discovery in metaproteomics. *Briefings Bioinf.* **2020**, *1*, No. bbaa105.
(42) Nightingale, B.; Dersch, C. M.; Boos, T. L.; Greiner, E.; Calhoun, W. J.; Jacobson, A. E.; Rice, K. C.; Rothman, R. B. Studies of the biogenic amine transporters. XI. Identification of a 1-[2-[bis(4-fluorophenyl)methoxy]ethyl]-4-(3-phenylpropyl)piperazine (GBR12909) analog that allosterically modulates the serotonin transporter. *J. Pharmacol. Exp. Ther.* **2005**, *314*, 906−915.
(43) Kortagere, S.; Fontana, A. C.; Rose, D. R.; Mortensen, O. V. Identification of an allosteric modulator of the serotonin transporter with novel mechanism of action. *Neuropharmacology* **2013**, *72*, 282−290.
(44) Larsen, M. A.; Plenge, P.; Andersen, J.; Eildal, J. N.; Kristensen, A. S.; Bogeso, K. P.; Gether, U.; Stromgaard, K.; Bang-Andersen, B.; Loland, C. J. Structure-activity relationship studies of citalopram

derivatives: examining substituents conferring selectivity for the allosteric site in the 5-HT transporter. *Br. J. Pharmacol.* **2016**, *173*, 925−936.
(45) Topiol, S.; Bang-Andersen, B.; Sanchez, C.; Bogeso, K. P. Exploration of insights, opportunities and caveats provided by the X-ray structures of hSERT. *Bioorg. Med. Chem. Lett.* **2016**, *26*, 5058−5064.
(46) Erol, I.; Aksoydan, B.; Kantarcioglu, I.; Salmas, R. E.; Durdagi, S. Identification of novel serotonin reuptake inhibitors targeting central and allosteric binding sites: A virtual screening and molecular dynamics simulations study. *J. Mol. Graph. Model.* **2017**, *74*, 193−202.
(47) Li, B.; Tang, J.; Yang, Q.; Li, S.; Cui, X.; Li, Y.; Chen, Y.; Xue, W.; Li, X.; Zhu, F. NOREVA: normalization and evaluation of MS-based metabolomics data. *Nucleic Acids Res.* **2017**, *45*, W162−W170.
(48) Xue, W.; Wang, P.; Tu, G.; Yang, F.; Zheng, G.; Li, X.; Li, X.; Chen, Y.; Yao, X.; Zhu, F. Computational identification of the binding mechanism of a triple reuptake inhibitor amitifadine for the treatment of major depressive disorder. *Phys. Chem. Chem. Phys.* **2018**, *20*, 6606−6616.
(49) Zhong, H.; Haddjeri, N.; Sanchez, C. Escitalopram, an antidepressant with an allosteric effect at the serotonin transporter–a review of current understanding of its mechanism of action. *Psychopharmacology* **2012**, *219*, 1−13.
(50) Plenge, P.; Shi, L.; Beuming, T.; Te, J.; Newman, A. H.; Weinstein, H.; Gether, U.; Loland, C. J. Steric hindrance mutagenesis in the conserved extracellular vestibule impedes allosteric binding of antidepressants to the serotonin transporter. *J. Biol. Chem.* **2012**, *287*, 39316−39326.
(51) Zhu, F.; Li, X. X.; Yang, S. Y.; Chen, Y. Z. Clinical success of drug targets prospectively predicted by in silico study. *Trends Pharmacol. Sci.* **2018**, *39*, 229−231.
(52) Niello, M.; Gradisch, R.; Loland, C. J.; Stockner, T.; Sitte, H. H. Allosteric Modulation of Neurotransmitter Transporters as a Therapeutic Strategy. *Trends Pharmacol Sci* **2020**, *41*, 446−463.
(53) Yang, Q.; Li, B.; Chen, S.; Tang, J.; Li, Y.; Li, Y.; Zhang, S.; Shi, C.; Zhang, Y.; Mou, M.; Xue, W.; Zhu, F. MMEASE: online meta-analysis of metabolomic data by enhanced metabolite annotation, marker selection and enrichment analysis. *J. Proteomics* **2021**, *232*, No. 104023.
(54) Hertig, S.; Latorraca, N. R.; Dror, R. O. Revealing Atomic-Level Mechanisms of Protein Allostery with Molecular Dynamics Simulations. *PLoS Comput. Biol.* **2016**, *12*, No. e1004746.
(55) Lv, Z.; Ao, C.; Zou, Q. Protein Function Prediction: From Traditional Classifier to Deep Learning. *Proteomics* **2019**, *19*, No. 1900119.
(56) Zhang, Y.; Zheng, G.; Fu, T.; Hong, J.; Li, F.; Yao, X.; Xue, W.; Zhu, F. The binding mode of vilazodone in the human serotonin transporter elucidated by ligand docking and molecular dynamics simulations. *Phys. Chem. Chem. Phys.* **2020**, *22*, 5132−5144.
(57) Li, Y. H.; Xu, J. Y.; Tao, L.; Li, X. F.; Li, S.; Zeng, X.; Chen, S. Y.; Zhang, P.; Qin, C.; Zhang, C.; Chen, Z.; Zhu, F.; Chen, Y. Z. SVM-Prot 2016: a web-server for machine learning prediction of protein functional families from sequence irrespective of similarity. *PLoS One* **2016**, *11*, No. e0155290.
(58) Tu, G.; Fu, T.; Yang, F.; Yang, J.; Zhang, Z.; Yao, X.; Xue, W.; Zhu, F. Understanding the Polypharmacological Profiles of Triple Reuptake Inhibitors by Molecular Simulation. *ACS Chem. Neurosci.* **2021**, *12*, 2013−2026.
(59) Park, S.; Khalili-Araghi, F.; Tajkhorshid, E.; Schulten, K. Free energy calculation from steered molecular dynamics simulations using Jarzynski's equality. *J. Chem. Phys.* **2003**, *119*, 3559−3566.
(60) Niu, Y.; Li, S.; Pan, D.; Liu, H.; Yao, X. Computational study on the unbinding pathways of B-RAF inhibitors and its implication for the difference of residence time: insight from random acceleration and steered molecular dynamics simulations. *Phys. Chem. Chem. Phys.* **2016**, *18*, 5622−5629.
(61) Do, P. C.; Lee, E. H.; Le, L. Steered Molecular Dynamics Simulation in Rational Drug Design. *J. Chem. Inf. Model.* **2018**, *58*, 1473−1482.
(62) Wang, E.; Sun, H.; Wang, J.; Wang, Z.; Liu, H.; Zhang, J. Z. H.; Hou, T. End-Point Binding Free Energy Calculation with MM/PBSA and MM/GBSA: Strategies and Applications in Drug Design. *Chem. Rev.* **2019**, *119*, 9478−9508.
(63) Du, Q.; Qian, Y.; Xue, W. Molecular Simulation of Oncostatin M and Receptor (OSM-OSMR) Interaction as a Potential Therapeutic Target for Inflammatory Bowel Disease. *Front. Mol. Biosci.* **2020**, *7*, No. 29.
(64) Du, Q.; Qian, Y.; Xue, W. Cross-reactivity of two human IL-6 family cytokines OSM and LIF explored by protein-protein docking and molecular dynamics simulation. *Biochim. Biophys. Acta, Gen. Subj.* **2021**, *1865*, No. 129907.
(65) Tang, J.; Fu, J.; Wang, Y.; Luo, Y.; Yang, Q.; Li, B.; Tu, G.; Hong, J.; Cui, X.; Chen, Y.; Yao, L.; Xue, W.; Zhu, F. Simultaneous improvement in the precision, accuracy, and robustness of label-free proteome quantification by optimizing data manipulation chains. *Mol. Cell. Proteomics* **2019**, *18*, 1683−1699.
(66) Yang, Q.; Hong, J.; Li, Y.; Xue, W.; Li, S.; Yang, H.; Zhu, F. A novel bioinformatics approach to identify the consistently well-performing normalization strategy for current metabolomic studies. *Briefings Bioinf.* **2020**, *21*, 2142−2152.
(67) Sørensen, L.; Andersen, J.; Thomsen, M.; Hansen, S. M.; Zhao, X.; Sandelin, A.; Stromgaard, K.; Kristensen, A. S. Interaction of antidepressants with the serotonin and norepinephrine transporters: mutational studies of the S1 substrate binding pocket. *J. Biol. Chem.* **2012**, *287*, 43694−43707.
(68) Zhu, F.; Qin, C.; Tao, L.; Liu, X.; Shi, Z.; Ma, X.; Jia, J.; Tan, Y.; Cui, C.; Lin, J.; Tan, C.; Jiang, Y.; Chen, Y. Clustered patterns of species origins of nature-derived drugs and clues for future bioprospecting. *Proc. Natl. Acad. Sci. U.S.A.* **2011**, *108*, 12943−12948.
(69) Fu, J.; Tang, J.; Wang, Y.; Cui, X.; Yang, Q.; Hong, J.; Li, X.; Li, S.; Chen, Y.; Xue, W.; Zhu, F. Discovery of the consistently well-performed analysis chain for SWATH-MS based pharmacoproteomic quantification. *Front. Pharmacol.* **2018**, *9*, No. 681.
(70) Gumbart, J. C.; Roux, B.; Chipot, C. Standard binding free energies from computer simulations: What is the best strategy? *J. Chem. Theory Comput.* **2013**, *9*, 794−802.
(71) Shi, L.; Quick, M.; Zhao, Y.; Weinstein, H.; Javitch, J. A. The mechanism of a neurotransmitter:sodium symporter–inward release of Na+ and substrate is triggered by substrate in a second binding site. *Mol. Cell* **2008**, *30*, 667−677.
(72) Hollingsworth, S. A.; Dror, R. O. Molecular Dynamics Simulation for All. *Neuron* **2018**, *99*, 1129−1143.
(73) Plenge, P.; Abramyan, A. M.; Sorensen, G.; Mork, A.; Weikop, P.; Gether, U.; Bang-Andersen, B.; Shi, L.; Loland, C. J. The mechanism of a high-affinity allosteric inhibitor of the serotonin transporter. *Nat. Commun.* **2020**, *11*, No. 1491.
(74) Plenge, P.; Yang, D.; Salomon, K.; Laursen, L.; Kalenderoglou, I. E.; Newman, A. H.; Gouaux, E.; Coleman, J. A.; Loland, C. J. The antidepressant drug vilazodone is an allosteric inhibitor of the serotonin transporter. *Nat. Commun.* **2021**, *12*, No. 5063.
(75) Capelli, A. M.; Bruno, A.; Entrena Guadix, A.; Costantino, G. Unbinding pathways from the glucocorticoid receptor shed light on the reduced sensitivity of glucocorticoid ligands to a naturally occurring, clinically relevant mutant receptor. *J. Med. Chem.* **2013**, *56*, 7003−7014.
(76) Mansari, M. E.; Wiborg, O.; Mnie-Filali, O.; Benturquia, N.; Sanchez, C.; Haddjeri, N. Allosteric modulation of the effect of escitalopram, paroxetine and fluoxetine: in-vitro and in-vivo studies. *Int. J. Neuropsychopharmacol.* **2007**, *10*, 31−40.
(77) Sanchez, C.; Reines, E. H.; Montgomery, S. A. A comparative review of escitalopram, paroxetine, and sertraline: Are they all alike? *Int. Clin. Psychopharmacol.* **2014**, *29*, 185−196.
(78) Loland, C. J.; Sanchez, C.; Plenge, P.; Bøgesø, K. P.; Bang-Andersen, B. Allosteric Binding in the Serotonin Transporter − Pharmacology, Structure, Function and Potential Use as a Novel Drug Target. In *Allosterism in Drug Discovery*; The Royal Society of Chemistry, 2017; Chapter 16, pp 360−380.

(79) Topiol, S.; Bang-Andersen, B.; Sanchez, C.; Plenge, P.; Loland, C. J.; Juhl, K.; Larsen, K.; Bregnedal, P.; Bogeso, K. P. X-ray structure based evaluation of analogs of citalopram: Compounds with increased affinity and selectivity compared with R-citalopram for the allosteric site (S2) on hSERT. *Bioorg. Med. Chem. Lett.* **2017**, *27*, 470−478.
(80) Cheng, M. H.; Bahar, I. Monoamine transporters: structure, intrinsic dynamics and allosteric regulation. *Nat. Struct. Mol. Biol.* **2019**, *26*, 545−556.
(81) Brinkø, A.; Larsen, M. T.; Koldso, H.; Besenbacher, L.; Kolind, A.; Schiott, B.; Sinning, S.; Jensen, H. H. Synthesis and inhibitory evaluation of 3-linked imipramines for the exploration of the S2 site of the human serotonin transporter. *Bioorg. Med. Chem.* **2016**, *24*, 2725−2738.
(82) Vatansever, S.; Schlessinger, A.; Wacker, D.; Kaniskan, H. U.; Jin, J.; Zhou, M. M.; Zhang, B. Artificial intelligence and machine learning-aided drug discovery in central nervous system diseases: State-of-the-arts and future directions. *Med. Res. Rev.* **2021**, *41*, 1427−1473.
(83) Mortensen, O. V.; Kortagere, S. Designing modulators of monoamine transporters using virtual screening techniques. *Front. Pharmacol.* **2015**, *6*, No. 223.
(84) Maier, J. A.; Martinez, C.; Kasavajhala, K.; Wickstrom, L.; Hauser, K. E.; Simmerling, C. ff14SB: Improving the Accuracy of Protein Side Chain and Backbone Parameters from ff99SB. *J. Chem. Theory Comput.* **2015**, *11*, 3696−3713.
(85) Dickson, C. J.; Madej, B. D.; Skjevik, A. A.; Betz, R. M.; Teigen, K.; Gould, I. R.; Walker, R. C. Lipid14: The Amber Lipid Force Field. *J. Chem. Theory Comput.* **2014**, *10*, 865−879.
(86) Wang, J.; Wolf, R. M.; Caldwell, J. W.; Kollman, P. A.; Case, D. A. Development and testing of a general amber force field. *J. Comput. Chem.* **2004**, *25*, 1157−1174.
(87) Bayly, C. I.; Cieplak, P.; Cornell, W. D.; Kollman, P. A. A Well-Behaved Electrostatic Potential Based Method Using Charge Restraints for Deriving Atomic Charges - the Resp Model. *J. Phys. Chem. A* **1993**, *97*, 10269−10280.
(88) Kollman, P. A.; Massova, I.; Reyes, C.; Kuhn, B.; Huo, S.; Chong, L.; Lee, M.; Lee, T.; Duan, Y.; Wang, W.; Donini, O.; Cieplak, P.; Srinivasan, J.; Case, D. A.; Cheatham, T. E., 3rd. Calculating structures and free energies of complex molecules: combining molecular mechanics and continuum models. *Acc. Chem. Res.* **2000**, *33*, 889−897.
(89) Zheng, G.; Xue, W.; Wang, P.; Yang, F.; Li, B.; Li, X.; Li, Y.; Yao, X.; Zhu, F. Exploring the Inhibitory Mechanism of Approved Selective Norepinephrine Reuptake Inhibitors and Reboxetine Enantiomers by Molecular Dynamics Study. *Sci. Rep.* **2016**, *6*, No. 26883.
(90) Wang, P.; Fu, T.; Zhang, X.; Yang, F.; Zheng, G.; Xue, W.; Chen, Y.; Yao, X.; Zhu, F. Differentiating physicochemical properties between NDRIs and sNRIs clinically important for the treatment of ADHD. *Biochim. Biophys. Acta, Gen. Subj.* **2017**, *1861*, 2766−2777.

https://doi.org/10.1021/acschemneuro.1c00694
ACS Chem. Neurosci. 2022, 13, 340−351